Received: 14 October 2019 | Revised: 13 July 2020 | Accepted: 23 September 2020

DOI: 10.4218/etrij.2019-0475

ORIGINAL ARTICLE

ETRI Journal WILEY

Implementation of platform for long-term evolution cell perspective resource utilization analysis

Jungsun Um | **Igor Kim** | **Seungkeun Park**

Radio Resource Research Team, Electronics and Telecommunications Research Institute, Daejeon, Rep. of Korea

Correspondence
Jungsun Um, Radio Resource Research Team, Electronics and Telecommunications Research Institute, Daejeon, Rep. of Korea.
Email: korses@etri.re.kr

Funding information
This work was supported by an Institute of Information & Communications Technology Planning & Evaluation (IITP) grant funded by the Korea government (MSIT) (2017-0-00109, Development of Frequency Analysis Technology for the Virtuous Circulation of Radio Resource).

Abstract

As wireless communication continues to develop in limited frequency resource environments, it is becoming important to identify the state of spectrum utilization and predict the amount needed in future. It is essential to collect reliable information for data analysis. This paper introduces a platform that enables the gathering of the scheduling information of a long-term evolution (LTE) cellular system without connecting to the network. A typical LTE terminal can confirm its assigned resource information using the configuration parameters delivered from a network. However, our platform receives and captures only the LTE signal over the air and then enables the estimation of the data relevant to scheduling for all terminals within an LTE cell. After extracting the control channel signal without loss from all LTE subframes, it detects valid downlink control information using the proposed algorithm, which is based on the error vector magnitude of depatterned symbols. We verify the reliability of the developed platform by comparing it with real data from mobile phones and service operators. The average difference in resource block utilization is only 0.28%.

KEYWORDS

analyzer, downlink control information, implementation, long-term evolution, resource blocks

1 | INTRODUCTION

Wireless data traffic is expected to increase with the emergence of new and high growth applications such as high-density (4K/8K) video and augmented reality/virtual reality services, in addition to short messages, digital images, video calls, and Internet access [1,2]. Accordingly, the capacity of wireless channels in mobile communication systems has also been expanded in both the spatial and frequency domains to accommodate the expected exponential growth of traffic [3]. With respect to the expansion of bandwidth, long-term evolution (LTE) in fourth-generation (4G) networks can aggregate up to five component carriers in a licensed spectrum with a single bandwidth of up to 20 MHz [4,5]. For new radio (NR) in fifth-generation (5G) networks, apart from carrier aggregation, larger frequency blocks are available that are 100 MHz wide below the 7 GHz band and up to 400 MHz wide at the high-frequency range of mmWave [6]. Another approach is to use the unlicensed bands or shared bands based on cognitive radio technologies under the frequency sharing framework for the purpose of data offloading, although resources cannot be used exclusively [7,8]. The supply of additional spectrum is the most reliable and effective solution, but there is also a need to ensure that the limited spectral resources are appropriately allocated to various applications and efficiently utilized. In addition, the price of

license spectrum auctions is comparable to the value of radio resources [9]. Therefore, mobile service providers (MSPs) initially attempt to effectively exploit the available frequency capacity before finally expanding the total bandwidth [10]. In this context, the utilization of multiple antenna schemes and the increase in the density of cells per unit area are typically considered [11,12]. Notably, there has been significant research activity on multiple antenna transmission schemes that can maximize spatial multiplexing gain for specific frequency resource conditions [13,14]. However, the configured number of antennas applied in the real field is relatively low compared with the maximum specified condition, which is insufficient to achieve the theoretical performance gain [15]. In practice, the reduction in cell size using approaches such as cell splitting has been widely exploited [16,17]. It allows the network capacity to be enhanced until the effects of mutual interference from adjacent cells can be tolerated [18]. Cell expansion can be conducted once the resource utilization ratio of a cell reaches a specific saturation criterion based on the threshold defined by each MSP [19,20]. Therefore, it is important to monitor the utilization of the assigned spectrum and observe the collected data, as in several recent data-based research analyses [21,22]. In particular, if detailed scheduling information of the resource allocation unit is collected, it can be used to analyze the cell statistical characteristics and develop a cell management prediction model. Even from a regulatory domain perspective, the dataset on resource utilization and its analyzed results can be extensively exploited to estimate frequency resource requirements and to manage the spectrum, including supply, retrieval, or rearrangement at the appropriate time depending on the usage rate of the resource. Moreover, in the upcoming era of spectrum sharing frameworks such as spectrum pooling, the technology to monitor the usage of other operators may become increasingly pertinent with respect to sharing common resources among heterogeneous operators [23]. However, such data are not easy to obtain autonomously and actively because they consist of information related to the private network operation of mobile operators. Therefore, it is necessary to collect the signals transmitted by the communication entities and extract and analyze the data [24]. To do this, it is necessary to have a platform to gather the desired data by considering the communication protocol of the wireless communication system and the receiving device, including the antenna of the wireless communication device [25].

In this paper, we introduce a platform called ALTETRI (Analyzer of LTE Traffic and Radio Information) that can gather scheduling information from all downlink control information (DCI) transmitted from an LTE base station denoted as eNodeB (eNB) [26]. Because the element fields in the DCI of LTE include the resource allocation information, traffic amount, and data transmission methods, it is possible to analyze the state of traffic and resource utilization of LTE networks if we can make use of a dataset of DCI. However, whereas a normal mobile device is sent the parameter necessary to receive DCI from the network in advance, the development platform should be able to acquire information by itself from the signals received over the air without any communication with the network. Therefore, we implement a receiver to save all control signals that exist every 1 ms of the LTE subframe and propose a reliable algorithm to derive valid DCIs based on the error vector magnitude of the depatterned symbol from the saved signals. To verify the operation of the platform, we compared the results of the average resource utilization with data extracted from a commercial smartphone and data provided by a mobile network operator.

The rest of this paper is organized as follows. Section 2 describes previous work and illustrates the LTE specification related to the development platform on the resource structure of the physical control channel and the decoding procedure for the DCI format. Section 3 presents the comprehensive platform and describes the architecture, functionality, and an algorithm for detecting valid DCIs. This section provides details on (1) the functional components within the platform, (2) the protocol for communication between the LTE signal receiver and graphical user interface, and (3) the methodology of detecting valid DCIs with its algorithm and flowchart. In Section 4, it is shown that the result of resource utilization measured by the platform is only a difference of 0.28% when compared with the data from a network operator. In addition, we provide analysis instances using measured datasets in this section. Finally, Section 5 presents our conclusions.

2 | RELATED WORK AND LTE SPECIFICATION

2.1 | Previous work

The 4G and 5G mobile communication systems transmit user traffic in multiple units of resource blocks (RBs) consisting of a plurality of subcarriers based on orthogonal frequency division multiplexing (OFDM) within a single operating bandwidth depending on factors such as the traffic demand, number of users, or scheduling capacity. Thus, once the occupied RBs can be estimated, it is also possible to identify the spectral usage status. One approach for identifying the RBs used for data transmission is to measure the radio signal strength or spectrum in the frequency domain. However, it is noted that it is not easy to accurately determine these parameters because they change dynamically with each scheduling unit of 1-ms subframe. As a possible alternative for acquiring information on resource utilization [27] first introduced LTEye, which can extract per-user analytics based only on the LTE control channels. eNB in a cell of the LTE

network informs user equipment (UE) scheduling information of granted resources by broadcasting DCI. Each UE can decode DCI by identifying an indicator, radio network temporary identifier (RNTI), configured by a higher layer. Without accessing the private data or system parameters from encrypted data channels, LTEye facilitates LTE radio analytics by detecting RNTI and decoding all possible DCIs in an LTE subframe. To improve valid DCI extraction performance, [28,29] have proposed improved algorithms based on ref. [27]'s algorithm. In ref. [28], two steps of detection and management of candidate RNTIs are applied. However, the threshold needs to be optimized in terms of determining valid DCI or RNTI under the various channel environments in the real field. In ref. [29], the response message broadcasted from eNB in the random access procedures is exploited as a supplementary method for increasing reliability. It arises due to the accompanying requirements for implementing protocols and increasing computational complexity for turbo decoding signal processing. In addition, when a secondary component carrier or secondary cell is observed for the carrier aggregation framework of the LTE-advanced (LTE-A) network, the random access response message cannot be received because it is delivered on a primary component carrier. Furthermore, all previous works used Universal Software Radio Peripheral (USRP) to receive an LTE signal. Even though it is very suitable for general purposes because it is specified in a soft defined radio system, synchronization may be degraded for measurements that are longer than a few seconds [29]. The authors experienced the loss of some subframes during actual measurements. Commercial instruments such as those in refs. [30] and [31] are available. However, [30] requires a segmented processing time for detecting DCI after capturing the signal using a spectrum analyzer, and only works well in a single cell environment. Even though [31] is available in a real environment, it only provides statistical data on sampled subframes for which exact numbers and durations are uncontrollable by the user. Therefore, we have implemented an FPGA-based hardware module to receive a secure and continuous LTE signal that reliably operates in an urban area with high cell density.

2.2 | Resources of control channel in LTE

A subframe of LTE downlink in the time domain is sequentially composed of a control region for broadcasting physical control information and a data region for transmitting user traffic, as shown in Figure 1. Three physical control channels, Physical Control Format Indicator Channel (PCFICH), Physical Hybrid-ARQ Indicator Channel (PHICH), and Physical Downlink Control Channel (PDCCH), are multiplexed in a control region with one, two, or three OFDM symbols, of which the number N_{Sym} is provided to UEs by the control format indicator (CFI) carried on PCFICH in every subframe. The value of CFI can be changed from one subframe to the next depending on the density of users in a cell.

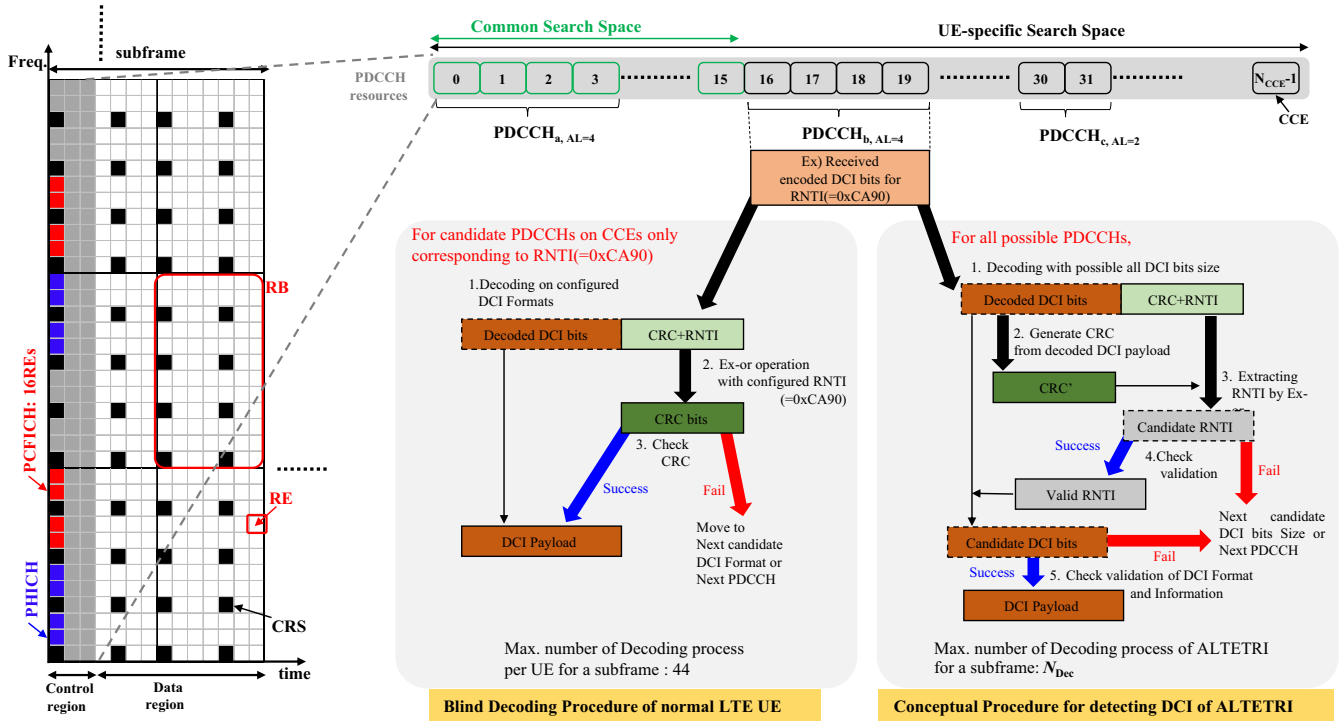

FIGURE 1 Illustrations of (A) resource structure in a subframe of LTE, (B) relation between CCE and PDCCH, and common and UE-specific search space for monitoring PDCCHs, and (C) procedure of blind decoding and conceptual procedure of ALTETRI and [27] when PDCCH_b is intended for UEs for which RNTI is 0xCA90

PCFICH uses 16 fixed number of resource elements (REs) on the first OFDM symbol in a subframe. PHICH carries a positive or negative acknowledgment (ACK/NACK) upon successful reception of uplink transport blocks sent over the physical uplink shared channel (PUSCH). The capacity of PHICH can be represented as the number of PHICH groups of $N_{\text{Group}}^{\text{PHICH}}$. It is determined as a function of the number of total RBs, $N_{\text{RB}}^{\text{BW}}$, for the downlink channel bandwidth and PHICH group scaling factor, $N_{\text{H}} \in [1/6, 1/2, 1, 2]$, that are informed via the master information block on the physical broadcast channel (PBCH) [32].

$$N_{\text{Group}}^{\text{PHICH}} = \left\lceil N_{\text{H}} \left(\frac{N_{\text{RB}}^{\text{BW}}}{8} \right) \right\rceil, \quad (1)$$

where $\lceil \cdot \rceil$ is the *ceiling* function. A PHICH group allocates a set of 12 REs that are divided into three quadruplets. PDCCH oversees the conveying of the DCI that schedules information of either downlink or uplink to be granted for UEs. After assigning REs for a common reference signal (CRS), PCFICH, and PHICH, the remaining REs in the control region are used to construct PDCCH. The basic resource unit for the PDCCH is the control channel element (CCE) that consists of nine resource element groups (REGs). Each REG contains four REs. A PDCCH can be assigned with one, two, four, or eight CCEs, defined as the aggregation level (AL). eNB can determine AL for the PDCCH according to the control information type or channel condition of the UE. The total number of CCEs, N_{CCE}, is as follows [32].

$$N_{\text{CCE}} = \left\lfloor \frac{N_{\text{RB}}^{\text{BW}} \cdot \left(12 \cdot N_{\text{Sym}} - N_{\text{CRS}}^{\text{AP}}\right) - 12 \cdot N_{\text{Group}}^{\text{PHICH}} - 16}{36} \right\rfloor, \quad (2)$$

where $N_{\text{CRS}}^{\text{AP}}$ is the total number of REs required for CRS depending on the antenna port in the PDCCH region, and $\lfloor \cdot \rfloor$ is the *floor* function. The maximum number of candidate PDCCHs is calculated by considering AL as follows:

$$N_{\text{PDCCH}} = \sum_{i=0}^{3} \left\lfloor N_{\text{CCE}} / (2^i) \right\rfloor. \quad (3)$$

Table 1 shows both N_{CCE} and N_{PDCCH} for the combination of conditions of the antenna port, N_{Sym}, and the bandwidths of 10 MHz and 20 MHz.

2.3 | Downlink control information in LTE

There are a variety of DCI formats defined according to the link direction (uplink/downlink) and a transmission scheme for data traffic [33]. DCI format 0 is for the uplink of PUSCH in one cell. DCI formats 1, 1A, 1C, 1D, 2, 2A, 2B, 2C, and 2D are used to schedule RBs for PDSCH and to inform the transmission process of PDSCH, such as the modulation order and precoding matrix. For reference, DCI formats 3 and 3A are defined for power control of the uplink channel rather than scheduling. The series of formats 1x is for one PDSCH codeword and is defined differently depending on the payload size and the inclusion of either precoding information or the uplink power offset field. The series of formats 2x can support up to two PDSCH codewords and is defined differently according to the MIMO scheme. For reference, DCI formats 3 and 3A are defined for power control of the uplink channel rather than scheduling. The DCI payload length is different depending on the DCI format; however, one of the same formats may vary depending on the information field configured by the eNB for each UE. As an example, if a cross-carrier scheduling or a sounding reference signal (SRS) request is activated to a UE, the carrier indicator field (CIF) of 3 bits or the SRS request field of 1 bit is included in DCI format 0 or 1A, respectively. Given that the UE knows the DCI configuration information from the eNB in advance, it operates on the assumption of a single defined bit size per DCI format. In the channel decoding process, the UE can identify the valid scheduling information by checking the status of the CRC, which is masked with RNTI via the Ex-OR operation and attached to the DCI payload. Given that some RNTIs are dedicated to a particular UE, which is cell RNTI (C-RNTI), it can receive a valid DCI by decoding encoded bits and checking the CRC on the PDCCHs associated with its C-RNTI without additional information. This process is called "blind decoding" and is depicted in Figure 1. The UE should perform multiple blind decoding processes for the DCI formats configured on the possible PDCCHs. It is necessary to perform multiple decoding trials owing to the different rate matching procedures for accommodating encoded bits for the DCI payload with different lengths into the CCE(s) of each AL. In each subframe, the UE is required to perform a maximum of 44 blind decoding executions consisting of 12 in the common search space (CSS) and 32 in the UE-specific search space (USS) [32]. The USS for monitoring PDCCHs is determined by the CCE start position corresponding to

TABLE 1 Number of control channel elements and candidate PDCCH

Antenna port		2 Ant. port			4 Ant. port		
N_{Sym}		1	2	3	1	2	3
N_{CCE}	10 MHz	10	26	43	4	21	37
	20 MHz	20	54	87	9	43	76
N_{PDCCH}	10 MHz	18	48	80	7	39	69
	20 MHz	37	101	163	16	80	142

the C-RNTI and the AL. In contrast, ALTETRI has to perform numerous decoding executions because all candidate DCI payload lengths in every possible PDCCH, as shown in Table 1, can be a hypothesis of a valid DCI. If the number of candidate DCI lengths is N_{DCI}, the maximum number of trials for decoding the candidate DCI, N_{Dec}, can be $N_{DCI} \times N_{PDCCH}$. Furthermore, given that RNTI information is unusable, it is very important and necessary for an efficient and reliable algorithm to be developed for ALTETRI based on the conceptual procedure, as depicted in the right side flow of Figure 1.

3 | DEVELOPMENT OF ALTETRI

ALTETRI has been developed for the following purposes:

- Receiving LTE signals without subframe loss.
- Detecting DCI with high efficiency and reliability.

For the first purpose, we implemented an FPGA-based control channel receiver. It can stably operate and gather constellation symbols in PDCCH resources without subframe loss. For the second purpose, we minimized the trial for DCI decoding and utilized the effect of channel and noise to determine whether a candidate DCI is valid. More details are covered in Section 3.2. The supported DCI formats are 0, 1, 1A, 1B, 1C, 1D, 2, 2A, 2B, 2C, 2D, 3, and 3A of 3GPP released from 8 to 12.

3.1 | Architecture and functionality

This subsection presents the architecture of the ALTETRI platform. It is functionally divided into three units that include a control and monitoring unit (Unit 1), an LTE signal receiving unit (Unit 2), and a control information detecting unit (Unit 3), as depicted in Figure 2. Unit 1 controls the operation of the other two units and manages the dataset from both units. It also presents users of the platform with various information about the quality of the received LTE signal, and statistical results for the detected DCI datasets. Unit 2 represents the FPGA-based hardware component. It performs some portion of reception procedures on the UE side and saves all constellation symbols of PDCCH resources per subframe. The collected datasets are then formed for the status and IQdata packets and transferred to Unit 1 according to the protocol as depicted in Figure 3 Unit 3 detects all DCIs broadcast to all UEs within one cell without any RNTI information configured by the eNB. It was implemented in software to flexibly verify and refine the DCI detection algorithm. Currently, we are implementing the proven algorithms on FPGA-based hardware components that enable real-time

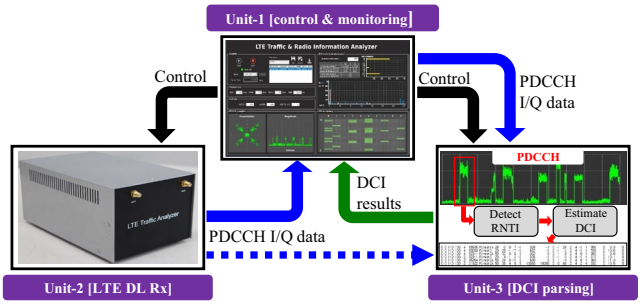

FIGURE 2 Three component units and their packet flow in the platform. Unit 1: Graphical user interface to control the platform and monitor results. Unit 2: Hardware device to receive the LTE signal and save the modulated signals of the control channel in every LTE subframe. Unit 3: Software tool for deriving valid DCIs with the proposed algorithm

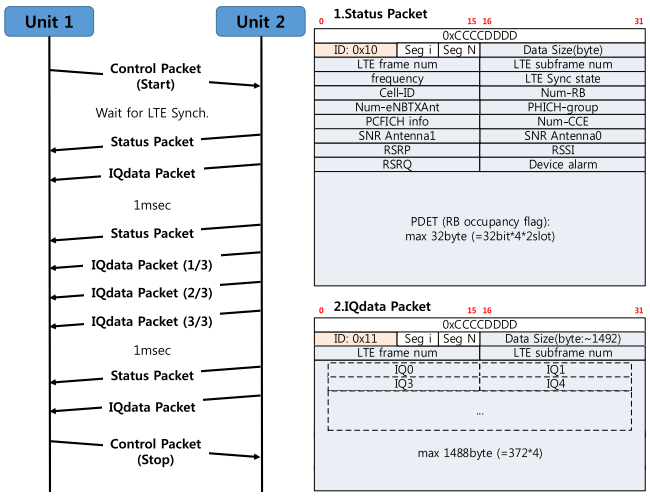

FIGURE 3 Protocol (left) and message format (right) between Unit 1 and Unit 2. Unit 1 requests to start or stop operation. Unit 2 transfers information on both the LTE signal quality and the cell, as well as PDCCH IQ data in every subframe

processing. From this point, we describe the implementation of Unit 2 and Unit 1, and then discuss the algorithm for Unit 3 in detail in the next subsection. Figure 4A shows the appearance of Unit 2, which is composed of two layers. The size is 22 cm × 13 cm × 11 cm, and the weight is 2 kg. The battery and the power distribution module are located in the lower layer. The battery provides flexibility when users measure the LTE signal in a real field, and its capacity is approximately 17 hours of operation. The upper layer consists of the RF board, FPGA, microcontroller unit (MCU), central processing unit (CPU), memory, and I/O interface. The role of each functional element and its interface is shown in Figure 4B. The radio-frequency (RF) board is equipped with an RF integrated circuit (IC) that supports LTE band numbers 1–41 and is connected to two antenna ports. Regardless of the number of antennas in eNB, the PDCCH can be decoded on the UE side with only one antenna port; therefore, the two

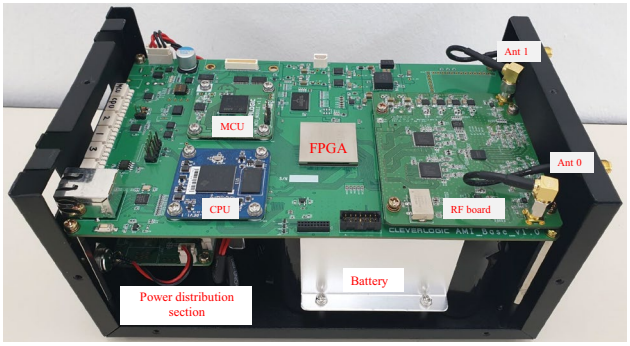

(A)

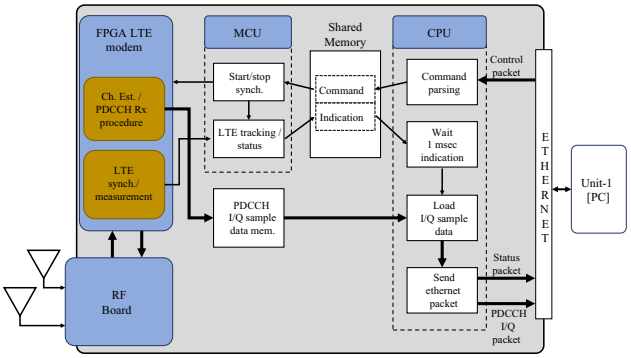

(B)

(C)

FIGURE 4 (A) Appearance of Unit 2 in ALTETRI. (B) Functionality and interface of Unit 2. (C) Snapshot of Unit 1

antenna ports are for 3 dB combined gain rather than MIMO reception. The dynamic range for the received signal is from −110 dBm to −10 dBm. The values of the parameters for the RFIC are controlled by the MCU using either the initial values from the CPU or the calibration values derived from the FPGA. Among the general reception model blocks of UE, LTE cell acquisition, synchronization, and channel estimation are implemented in the FPGA. In addition, a new block for gathering the I/Q constellation data on all CCEs for PDCCHs is included in it. In every subframe, it delivers cell information, signal quality information, and LTE tracking status to the MCU, and stores all I/Q samples of PDCCH resources in memory. The CPU receives measurement instructions from the user or forwards one status packet, and up to three PDCCH IQdata packets to Unit 1 per 1 ms subframe. The number of IQdata packets is determined by the bandwidth and CFI values.

A snapshot of the graphical user interface (GUI) in Unit 1 is shown in Figure 4C. The screen of the GUI is divided into four sections: the control, the received signal quality, the RB occupancy, and the DCI statistical information. In the first section, the user can examine the quality of all LTE signals received at the location of the ALTETRI through the "*SCAN*" function and then start or stop the measurement for the selected LTE cell. In the second section, the received LTE signal quality information such as RSRP, RSRQ, and SINR is expressed. In addition, the constellation and strength of the signal on the PDCCH resources during a subframe are provided. The RB occupancy state during 10 subframes is represented in the third section. The x- and y-axes represent the unit of the subframe in the time domain and the unit of RB in the frequency domain, respectively. The fourth region determines the statistical results analyzed by detected valid DCIs such as the average RB usage, MCS distribution, transmission rate, and DCI format ratio. The sample observation interval for deriving statistics can be specified by the user in the unit of subframes.

3.2 | New algorithm for detecting valid DCIs

ALTETRI must acquire scheduling information of DCI using only live LTE signals without being connected to the network. Therefore, compared to a conventional LTE terminal that performs blind decoding 44 times for each subframe, if ALTETRI does not know the network configuration information of other UEs in the cell, a large number of decoding operations are required. The main difficulty and complexity of the ALTETRI's operation are due to the absence of information on UEs configured from the network, for example, Radio Resource Control (RRC) configuration message and C-RNTI. The format and bit size required of DCIs for the UE to monitor the USS domain are determined based on the RRC message. The candidate CCE resources for the PDCCHs are associated with C-RNTI. Therefore, ALTETRI must perform all DCI format decoding on all possible PDCCHs and determine whether it is a valid DCI for a valid RNTI, as shown in Figure 1. Therefore, it is necessary to minimize the number of candidate PDDCHs by first determining the occupied CCEs and to reliably and effectively detect valid DCIs. The proposed algorithm is presented in Algorithm 1. In addition, its flowchart is shown in Figure 5, where the red dotted box indicates the step of confirming the occupied CCE, and the blue dotted box is the step of detecting the valid DCIs according to the ALs and DCI formats.

To minimize the computational complexity of the algorithm and to efficiently detect the signal, the CCE occupancy discrimination and fast DCI decision steps are introduced. In addition, a DCI detection step that considers channel

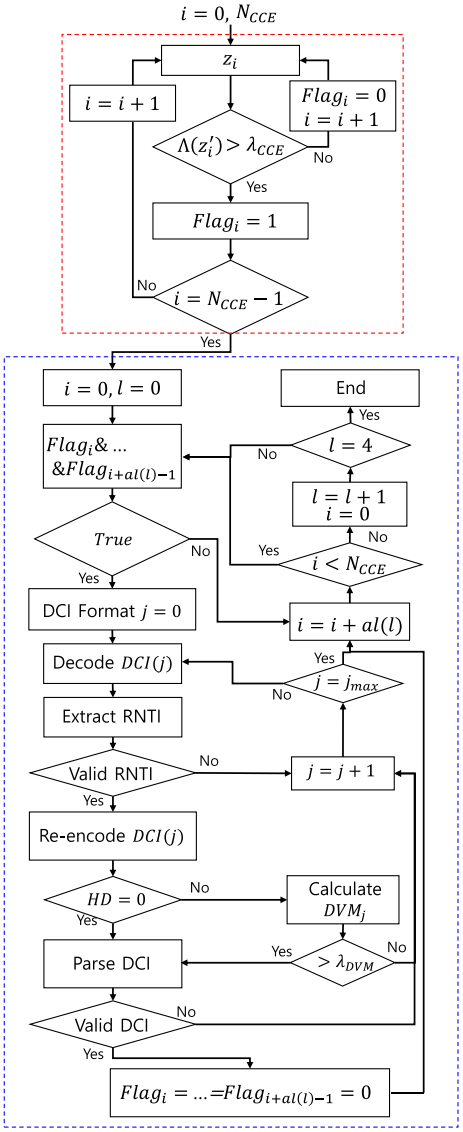

FIGURE 5 Flow chart of the algorithm that enables ALTETRI to detect the valid DCIs. As "$al(l)$" denotes the function of the aggregation level, it is defined that $al(0) = 8, al(1) = 4, al(2) = 2,$ and $al(3) = 1$. DCI(j) denotes the jth DCI format. Here, $j_{max} = N_{\text{DCI}}$

conditions is performed for reliable detection in a channel situation when a fast decision is not made. When a complex constellation symbol on the kth RE of the ith CCE is defined as $s_{i,k}$, the criterion for detection of the occupied CCE is based on a constant false alarm rate (CFAR) as follows [34].

$$z = \frac{1}{N_{\text{RE}}^{\text{CCE}}} \sum_{k=0}^{N_{\text{RE}}^{\text{CCE}}-1} s_{i,k} s_{i,k}^*, \tag{4}$$

$$\Lambda(z') = \frac{p(z'|H_1)}{p(z'|H_0)} = e^{\frac{2z'\mu - \mu^2}{2}} \underset{<}{>} \lambda_{\text{CCE}},$$
$$H_0: s = n, H_1: s = x + n, \tag{5}$$

where $N_{\text{RE}}^{\text{CCE}}$ is the number of REs in a single CCE, which is 36, and x and n are complex symbols of QPSK for DCI in PDCCH, and white Gaussian noise, respectively. μ is the expectation $E(z')$ for the hypothesis of H_1. Given the decision criterion of $z' = 10\log(z)$, when $\Lambda(z')$ exceeds the threshold λ_{CCE}, the ith CCE is determined to be occupied and Flag_i is set to one. Otherwise, Flag_i is set to zero.

In the case of H_0, the random variable of $s_{i,k}s_{i,k}^*$ is distributed as a noncentral chi-square with two degrees of freedom, and the random variable of z becomes a normal distribution considering the central limit theorem. Figure 6 is normalized histograms of the datasets that are measured by ALTETRI in the real field for 10 seconds. The gray bars in (a) and red bars in (b) are the density for $s_{i,k}s_{i,k}^*$ and z' for the condition of H_0. The blue bars are for z' in the condition of H_1, when the SINR of the LTE signal is approximately 15 dB. The four different bell-shaped distributions appear to be due to PDCCH boosting effects. Using $\ln\Lambda(z')$ in (5), the decision threshold becomes as follows.

$$z' \underset{<}{>} \lambda'_{\text{CCE}} = (2\lambda_{\text{CCE}} + \mu^2)/2\mu. \tag{6}$$

We set the value of λ'_{CCE} by using the LTE signal measured in the real field under the condition that the signal-to-noise

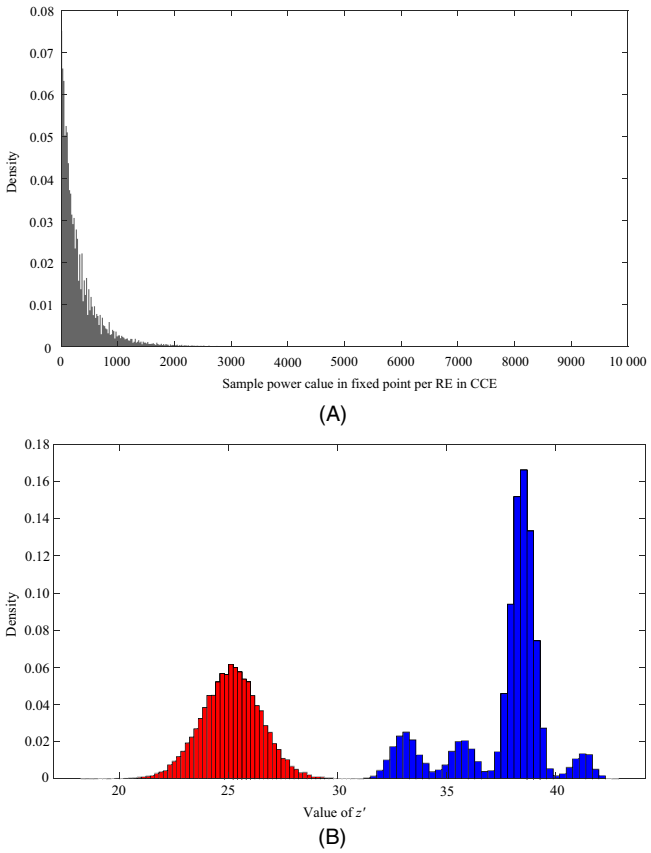

FIGURE 6 Histograms for (A) $s_{i,k}s_{i,k}^*$:H_0, (B) z': H_1 (blue) and z' :H_0(red)

ratio is approximately 5 dB. Given the threshold, we also confirmed that ALTETRI can detect all the system information block 1 (SIB1) of LTE, which is periodically broadcasted 512 times (10.24 s) during 1024 frames. It is noted that the eNB assigns the dedicated RNTI (=35 565) to DCI for SIB transmission. By adopting the detection of occupied CCEs, we can reduce the complexity and load of the process in Unit 3 and minimize the probability of false alarm detection for DCI under the condition of a larger AL containing unoccupied CCEs.

Algorithm 1

Load PDCCH data
Find out the number of CCEs of each subframe, N_{CCE}
Set "Flag" on each CCE, $Flag_i = 0$ or 1, $i = 0, \ldots, N_{CCE} - 1$
Decode candidate PDCCHs in the order of AL = 8, 4, 2, 1
if ($Flag_i$.& … &$Flag_{i+AL-1}$)=1 **then**
  for DCI Format j = {1A, 2, 2A, 1, 1C,…} **do**
    Decode received encoded-bits of $\boldsymbol{d}$
    Generate CRC bits
    Extract candidate RNTI from CRC bits
    Check whether candidate RNTI is valid
    if Valid RNTI **then**
      Re-encode the candidate DCI to $\tilde{\boldsymbol{d}}$
      Calculate hamming distance (= ***HD***) of $\boldsymbol{d}$ and $\tilde{\boldsymbol{d}}$
      if ***HD*** = *0* **then**
        Decide whether the candidate DCI is valid
        Update to next CCEs or next AL
      end if
      Calculate DVM_j
      Compare $-DVM_j$ with λ_{DVM}
      Update DCI Format list with larger DVM_j
    end if
  end for
  Confirm candidate DCI Format
  Check DCI
  if Valid DCI **then**
    $Flag_i = \ldots = Flag_{i+AL-1} = 0$
  end if
end if

After $Flag_i$s are set for all CCEs, the channel decoding trials are performed with the possible DCI sizes per each PDCCH of which AL is considered in the order of 8, 4, 2, and 1. DCI detection is attempted from larger AL values because it may be detected even at smaller values compared with AL used for actual transmission. When the capacity of CCE is sufficiently large to support the encoded DCI bit size, some of the encoded bits of DCI are repeatedly transmitted in the PDCCH due to the rate matching procedure based on the structure of the circular buffer. If DCI is detected in a smaller AL, this may lead to problems, such as either an incorrect DCI or an increase in the non-detection probability in the remaining CCEs.

To identify a candidate RNTI, it is assumed that there is no bit error in both the decoded DCI payload and the CRC portion. We can obtain CRC bits from the decoded DCI bits by using the generation function, and then, the candidate RNTI can be extracted from the portion of CRC in the received bits via Ex-OR operation with re-generated CRC bits. In the USS, given that the start index of CCEs for PDCCH varies according to the RNTI, validation of candidate RNTI can be identified using the CCE index. However, a check of the validation of RNTI for the CSS is not possible because all RNTIs allow PDCCH configuration in the CSS. Thus, in the case of the DCI formats 1A and 1C with AL as either 4 or 8 in the CCE index from 0 to 15, all candidate RNTIs remain as a valid status.

The next step in the development of an algorithm is to validate the DCI format (size) as a fast DCI decision step. Initially, the Hamming distance (*HD*) between the received codeword, d, and the re-encoded codeword, $\bar{d}$, is examined. If the *HD* is 0, then the DCI format is immediately determined to be valid. Otherwise, it is necessary to calculate the error vector magnitude of the depatterned symbols (DVM). The depatterned symbols and *DVM* are calculated using (7) and (8) [35].

$$p_{j,k} = s_{j,k}\,\tilde{x}^*_{j,k}, \tag{7}$$

where k and j represent the kth RE among the resources for the jth candidate DCI format on PDCCH. $s_{j,k}$ is the received symbol, and $\tilde{x}$ is a QPSK symbol that is modulated from re-encoded DCI bits.

$$\mathrm{DVM}_j = 10\log\left[\frac{P_{\mathrm{error}}}{P_{\mathrm{Refernce}}}\right] = 10\log\left[\frac{\mathrm{Var}(p_j)}{\mu_{p_j}\mu_{p_j^*}}\right], \tag{8}$$

where μ_{p_j} and $\mathrm{Var}(p_j)$ are the sample mean and sample variance for the depatterned symbols. Figure 7 shows the constellation points of the depatterned symbols and the mean value when correct and incorrect DCI formats are considered for the same candidate PDCCH. "Received Sym" and "Re-encoded Sym" represent s and $\tilde{x}$, respectively. If there is no error in the re-encoded DCI bits of the candidate DCI format, the depatterned signals converge to one point, and only the effect of noise is shown as in Figure 7A. If the candidate DCI format is incorrect for the current PDCCH, the depatterned symbols are scattered around four points as shown in Figure 7B. It is then defined to confirm whether the candidate DCI format is valid or not based on the following criterion:

$$-\mathrm{DVM}_j \underset{<}{\overset{>}{}} \lambda_{\mathrm{DVM}} = \min(\lambda_{\mathrm{SINR}} - \lambda_{\mathrm{DVM_{BO}}}, \lambda_{\mathrm{DVM_{min}}}), \tag{9}$$

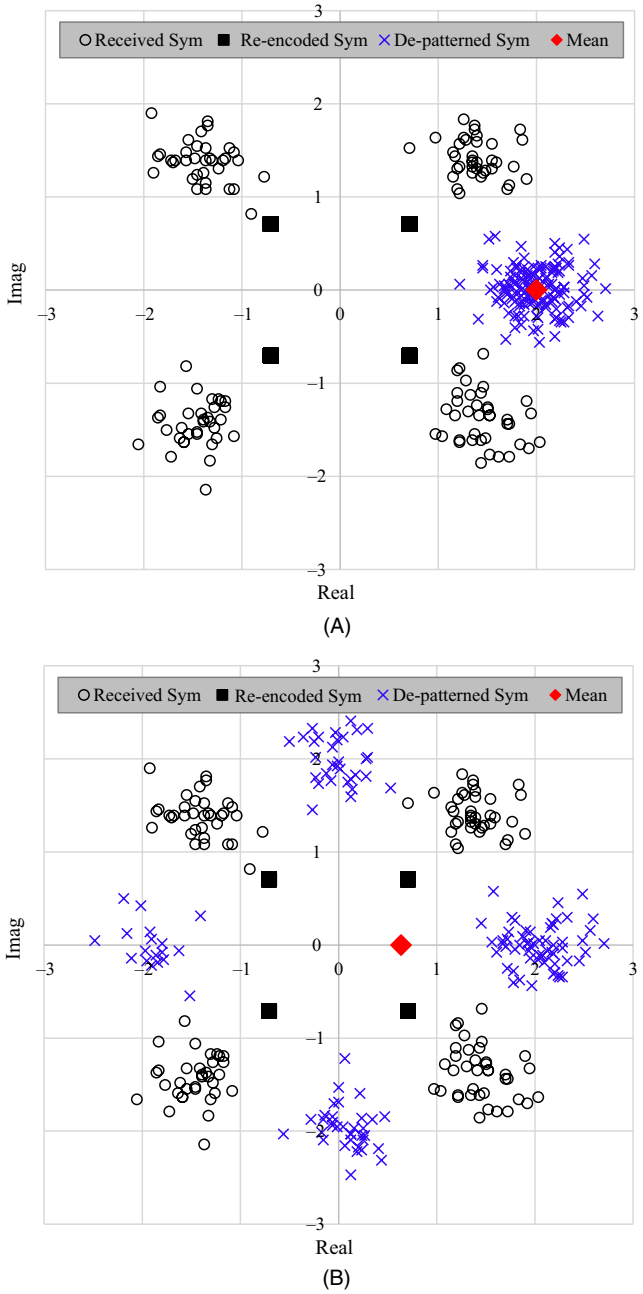

FIGURE 7 Constellation on s, $\tilde{x}$, p_j, and μ_{p_j} of (A) DCI format 1A (correct) and (B) DCI format 1 (incorrect) as considered for a candidate format when DCI format 1A is used for transmission

where λ_{SINR} is a SINR of the LTE signal measured over the air. In addition, $\lambda_{\text{DVM}_{\text{BO}}}$ and $\lambda_{\text{DVM}_{\text{min}}}$ are back-off values from SINR and the minimum threshold, respectively, to determine the valid DCI format. By utilizing λ_{SINR}, we can consider the channel environment during the measurement. If $-\text{DVM}_j$ exceeds the threshold, the jth candidate DCI format is ranked in the list of candidate formats based on the value of DVM_j. After all the formats are reviewed, the format with the highest ranking is chosen.

As a final state, we verified whether the values in the information field of DCI were valid. If the value of a certain field is not defined in the standard of ref. [33] or the "reserved" value is used, it is determined to be an invalid DCI. For example, when DCI format 1A is used in a random access procedure, all the specific fields must have a value of "0." In DCI format 2, "reserved" values cannot be received in the precoding matrix field. If all the conditions are satisfied, the DCI is finally determined to be valid, and all Flag_is of the CCE(s) are converted to a zero value. Then, the same process is executed for the next AL or the next PDCCH until an examination is complete for all occupied CCEs.

4 | VALIDATION AND ITS APPLICATION

This section presents the validation of operation and the measurement-based analysis examples for ALTETRI. To prove that ALTETRI correctly obtains DCIs from live LTE signals, we compared the scheduling information extracted from a commercial UE diagnostic monitoring tool (DMT) and ALTETRI. It should be noted that DMT gathers information from correct DCIs received on the LTE Modem Chipset in a UE. However, the important point is that these data are only for the single UE connected to DMT, rather than all UEs within an LTE cell. In contrast, ALTETRI should acquire information from control channels intended for all UEs that are communicating with the eNB. Therefore, we extract and compare only DCIs related to the UE connected to the DMT from the dataset collected by ALTETRI and compare them with the DMT output. Because the C-RNTI assigned for the UE is revealed in the output data from DMT, we can easily determine the desired DCIs by confirming the same C-RNTI in the whole dataset of ALTETRI measurement. Figure 8 shows the comparison results obtained from the data measured by the two at the same location. The DMT hexadecimal 0x594D has the same value as the ALTETRI's decimal 22 861. The figure shows the DCIs for the 15 subframes between radio frames 63 and 564. Because one radio frame becomes 10 ms with the 10 subframes, this indicates that the UE has been assigned the downlink resources 15 times during the approximately five seconds. With regard to MCS, which represents the modulation order and channel coding rate, both are the same, even though ALTETRI's result in Figure 8B represents the MCS index value of five bits, and DMT's result in Figure 8A shows only the modulation order. We can also confirm that the coding rates are matched because the TBS of the two results is the same. Here, TBS is the number of bit sizes to be transferred from eNB to UE, and it is derived from the number of RBs and the MCS index included in the DCI. In LTE, there can be up to two different transport blocks (TBs) consisting of both user traffic and control messages, which are denoted as stream 1 and stream 2 in Figure 8A. TBs can be delivered via multiple antennas to

[LTE] [TTI Level] [LL1 PDSCH Demapper Config] [PCell] SFN	[LTE] [TTI Level] [LL1 PDSCH Demapper Config] [PCell] sub-Fn	[LTE] [TTI Level] [LL1 PDSCH Demapper Config] [PCell] RNTI ID	[LTE] [TTI Level] [LL1 PDSCH Demapper Config] [PCell] TB Size for Stream 0 (bits)	[LTE] [TTI Level] [LL1 PDSCH Demapper Config] [PCell] TB Size for Stream 1 (bits)	[LTE] [TTI Level] [LL1 PDSCH Demapper Config] [PCell] Modulation for Stream 0	[LTE] [TTI Level] [LL1 PDSCH Demapper Config] [PCell] Modulation for Stream 1	[LTE] [TTI Level] [LL1 PDSCH Demapper Config] [PCell] RB Num Slot 0	[LTE] [TTI Level] [LL1 PDSCH Demapper Config] [PCell] Transmission Mode
63	4	0x594D	16	16	QPSK	QPSK	1	Closed-loop spatial multiplexing
191	2	0x594D	16	16	QPSK	QPSK	1	Closed-loop spatial multiplexing
289	3	0x594D	16	16	QPSK	QPSK	1	Closed-loop spatial multiplexing
415	3	0x594D	16	16	QPSK	QPSK	1	Closed-loop spatial multiplexing
513	4	0x594D	16	16	QPSK	QPSK	1	Closed-loop spatial multiplexing
539	9	0x594D	40	40	QPSK	QPSK	1	Closed-loop spatial multiplexing
540	2	0x594D	1,288	1,288	64QAM	64QAM	3	Closed-loop spatial multiplexing
545	0	0x594D	40	40	QPSK	QPSK	1	Closed-loop spatial multiplexing
548	7	0x594D	376	376	64QAM	64QAM	1	Closed-loop spatial multiplexing
551	0	0x594D	40	40	QPSK	QPSK	1	Closed-loop spatial multiplexing
554	9	0x594D	40	40	QPSK	QPSK	1	Closed-loop spatial multiplexing
557	0	0x594D	328	328	64QAM	64QAM	1	Closed-loop spatial multiplexing
560	1	0x594D	10,296	10,296	64QAM	64QAM	16	Closed-loop spatial multiplexing
560	5	0x594D	5,544	5,544	64QAM	64QAM	12	Closed-loop spatial multiplexing
564	0	0x594D	40	40	QPSK	QPSK	1	Closed-loop spatial multiplexing

(A)

Frame Idx	SF Idx	RNTI	DCI Format	TBS 1	TBS 2	MCS_1 Idx	MCS_2 Idx	# of RBs	CCE Start Idx
63	4	22861	Format2	16	16	0	0	1	12
191	2	22861	Format2	16	16	0	0	1	8
289	3	22861	Format2	16	16	0	0	1	12
415	3	22861	Format2	16	16	0	0	1	12
513	4	22861	Format2	16	16	0	0	1	12
539	9	22861	Format2	40	40	3	3	1	0
540	2	22861	Format2	1,288	1,288	21	21	3	2
545	0	22861	Format2	40	40	3	3	1	8
548	7	22861	Format2	376	376	20	20	1	12
551	0	22861	Format2	40	40	3	3	1	8
554	9	22861	Format2	40	40	3	3	1	0
557	0	22861	Format2	328	328	18	18	1	8
560	1	22861	Format2	10,296	10,296	27	27	16	14
560	5	22861	Format2	5,544	5,544	22	22	12	14
564	0	22861	Format2	40	40	3	3	1	8

(B)

FIGURE 8 When C-RNTI allocated to the tested UE is 0x594D(=22861), (A) snapshot of the GUI used for UE diagonal monitoring tool and (B) results for extracting DCI data only for C-RNTI of 22861 extracted from all measurements of ALTETRI

UE by using a MIMO scheme among the LTE transmission modes. In Figure 8B, DCI format 2 indicates a closed-loop spatial multiplexing method of Figure 8A in which a base station receives channel state information from a UE, and then determines and transmits a precoding matrix for MIMO. The results confirm that ALTETRI obtains the same information with the results of DMT for all elements in the DCI field.

In the real environment, however, because it is impossible to connect DMT to all terminals, all the cell information of LTE is difficult to obtain in the above DMT-based manner. Therefore, we have compared the measurement results by ALTETRI and the results that are limited but can be provided by the MSP. To align with the statistical conditions of the provided data, we analyzed the average RB utilization of the data measured for one hour. The measurement site is the area near Gangnam Station in Seoul, and we simultaneously received the signal of LTE cells operating at different center frequencies for four LTE bands, as shown in Figure 9A. The four bands are currently used for LTE service by one MSP, which provides relevant information to us. The measurements were performed six times at different dates and times in the same location. Figure 9B shows the analysis of the ALTETRI measurement as a circle and the MSP's data as dotted lines. For the convenience of data division, ALTETRI generated the file every 10.24 s for the data of 1024 radio frames and made the starting point of the collection the first index of the radio frame. Thus, some difference in the results may occur because of the offset of the start times of the comparative data. Nevertheless, the RBUs for both are almost consistent, and the average and variance of the difference between the two results are 0.28% and 0.098%, respectively. One of the things that can be seen in the resulting pattern is that Band A is the main service band of this MSP in the measurement area. Cases 5 and 6 were measured at busy times, when many users exist, and the RBU of Band A is larger than that of other bands. This means that the cell of Band A is mainly connected by the user devices because of its better connectivity and service quality.

Figure 10 shows a comparison results between ALTETRI and [28] for the RBU per radio frame. They both use the same IQ data of PDCCHs received from Unit 2 when the average RBU for the measured target cell is 97.5%. In ref. [28], it was highlighted that two- or 12-bit errors per CCE are required under optimum radio conditions or for a public eNB out of the office, respectively. The meaning of the bit error is the same *HD* in this paper. From the results, it is determined that the RBUs of the conventional algorithm vary significantly depending on the threshold. In addition, it is evident that there is a problem in that an RBU of more than 100% is detected at 4 bits or higher.

(A)

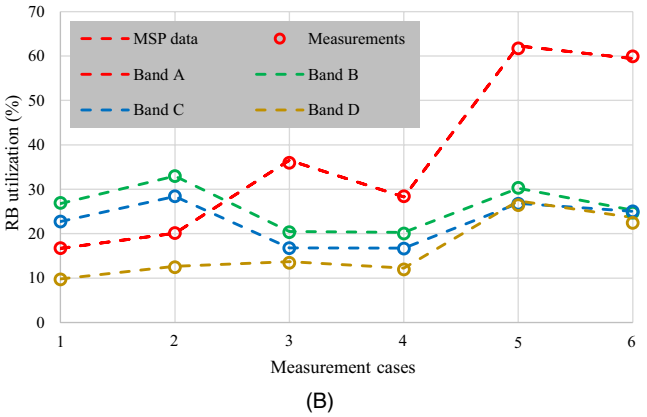

(B)

FIGURE 9 (A) Image for actual measurements near Gangnam Station. (B)Comparisons between the provided data from MSP (dash) and measured results (circle) for six measurements. Bands A, C, and D have a bandwidth of 10 MHz, whereas Band B has a bandwidth of 20 MHz

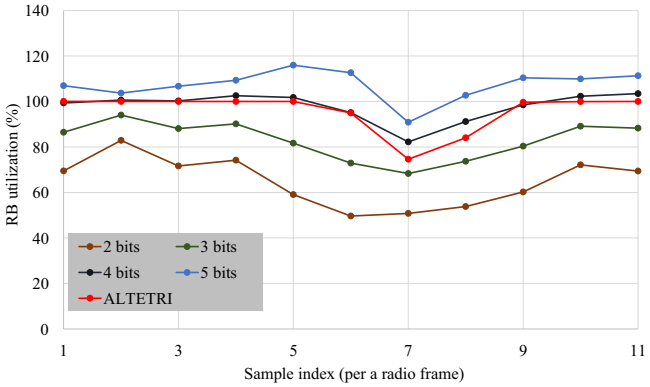

FIGURE 10 Comparison of the proposed and conventional algorithms. The number of bits is the threshold for the decision regarding valid DCI in the conventional approach

Figures 11–13 are typical results for cell operation and scheduling, which are analyzed from the measurement dataset for 10 MHz bandwidth cells in dense urban areas. Figure 11 shows the percentage usage of each value for CFI and AL in cells with different RB utilization (RBU). It was determined that CFI 3 and AL 8 were generally rarely used in practice and the three cells measured. For high RBU cells, even though the number of users was approximately 100, the number of DCIs transmitted per subframe via scheduling was kept below a certain value to avoid exceeding the capacity of the control channel; therefore, CFI 8 was not used. Considering the small cell coverage and the control channel capacity, it is expected that the AL of 8 would be rarely used; rather, the usage of AL of either 2 or 4 can be high. Figure 12 presents the distribution of the scheduling gap (SG) for a UE, which represents the interval scheduled in subframe units. In addition, Figure 13 shows the distribution of the number of RBs allocated per subframe to all UEs in Figure 12. Max UE, and 0.1% and 0.1% UE represent the UE with the highest RB utilization, and the UE that used 0.1% and 0.01% RB in the average RBU, respectively. When the RBU is below a medium of 46%, SG shows a similar pattern regardless of whether there are UEs with different amounts of required resources. If possible, it is analyzed to immediately

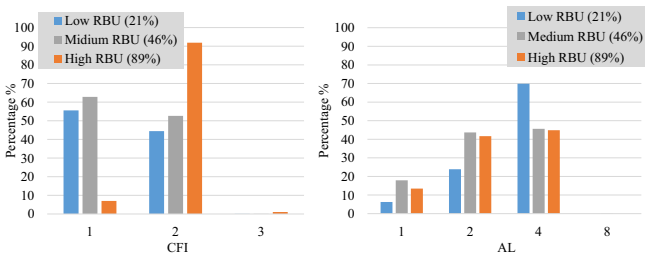

FIGURE 11 Percentage usage of aggregation level and control format indicator for three different cells for which RBU is low, medium, and high

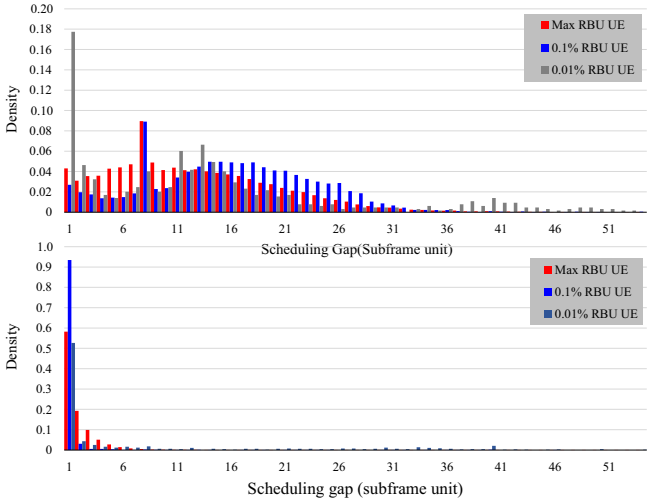

FIGURE 12 For the conditions of high (89%, top) and medium (46%, bottom) RBU, scheduling gap for UEs. Max, 0.1%, and 0.01% RBU UE indicate the UE using the highest number of RBs, that using 0.1% of the total RBs, and that using 0.01% of the total RBs, respectively

allocate as many as 50 RBs resources, as shown in Figure 13, whenever there is a demand for traffic transmission. In contrast, for the condition where the RBU is as high as 89%, it has different distribution characteristics according to the user traffic. Given that the resources are nearly saturated, the interval allocated to the UEs is relatively well spread. It is noted that the peaks on the SG value of 8 for Max and 0.1% UE are due to retransmission. In addition, the retransmission rate for all UEs was approximately 10%. In the case of 0.01% UE, a small RB is multiplexed with another UE or a large RB is scheduled with a large SG. Given the collected data, as shown in Figures 12 and 13, it is expected that it may be used to analyze the scheduling scheme of the eNB or for its optimization according to the operational requirements of the UEs.

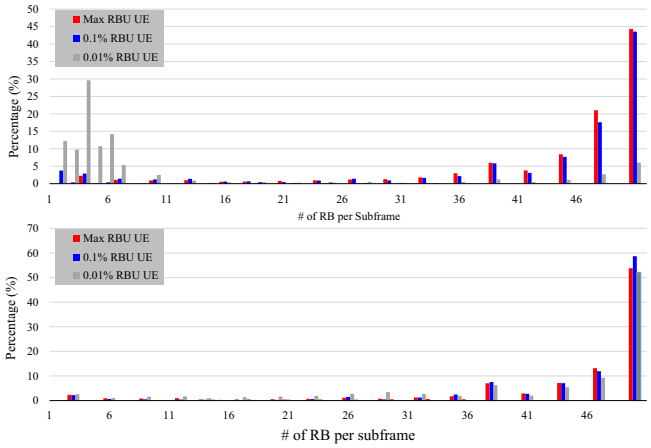

FIGURE 13 For the condition of high (89%, top) and medium (46%, bottom) RBU, the distribution of the number of allocated RBs to UEs

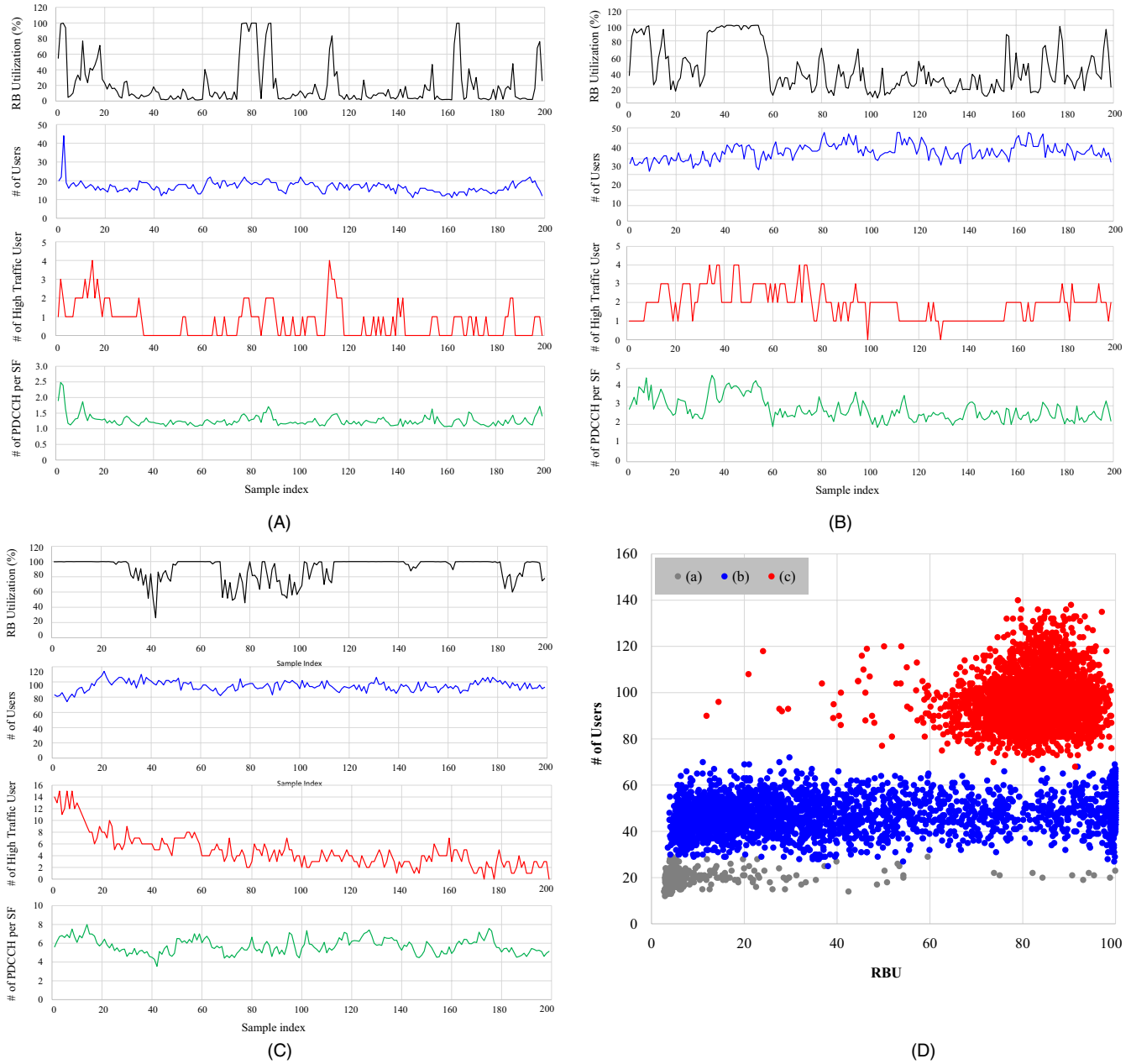

FIGURE 14 Analysis of the measured dataset for three different LTE cells with an average RBU of (A) 20%, (B) 50%, and (C) 90% and (D) scatter plot of RBU vs number of users per LTE subframe

Figure 14 shows analysis examples on the dataset measured from three LTE cells for which the average RBUs are not the same. Each cell operates with the same 20 MHz bandwidth of the same center frequency but at a different location. Figure 14A–14C shows cells with an average RBU of 20%, 50%, and 90% for 1 hour, as low, middle, and high RBU, respectively. To investigate the factors that affect the RBU, we examined the number of users $\overline{N}_{\text{user}}$, the number of users with more than 1 Mbps data traffic $\overline{N}_{\text{HTuser}}$, and the number of PDCCHs $\overline{N}_{\text{PDCCH}}$ per subframe for an average of 1-s duration. The number of valid RNTIs detected during one second is defined as $\overline{N}_{\text{user}}$. The results show that the average RBU is proportional to the average number of users. This can be explicitly confirmed with $\overline{N}_{\text{user}}$ versus RBU in Figure 14D for the case of low and high average RBU. In the case of an average RBU of 50%, the number of used RBs varies from 0 to whole RB according to the number of users activating instantaneously and their traffic. In a given dataset, it is expected that the threshold of the number of affordable users would be in the range of 60–80 because it is difficult to accommodate new users because of the deficit of resources when the average RBU is over 90%. It can be seen that the cell in Figure 14C is saturated because of the large number of users. Therefore, it may be determined that cell division or expansion is necessary. In fact, there are other

unused LTE frequency bands of MSP to be newly deployed in the area where the cell in Figure 14C is located. However, if there are no available channels or if the interference from the neighboring cell has already exceeded the allowable threshold, it should be assumed that additional spectrum resources are urgently needed.

5 | CONCLUSIONS

In this paper, we discussed the implementation, architecture, and algorithm of the ALTETRI platform that collects all scheduling information from the LTE downlink control channel. Because it is not connected to a mobile network that delivers the configuration information required to decode the DCI, it is necessary to minimize the complexity for detecting valid DCIs under many candidate hypotheses. Furthermore, it should operate while being adaptable to the channel environment because it measures the real field signal in various operating circumstances. To reduce the number of trials for decoding, the platform initially examines the status of occupancy in the candidate control channels as the first step. In addition, the decoding test sequence for aggregation level and DCI formats, which are parameters to be considered for the detection of DCI, was optimized. Regarding the measurement environment, we set the threshold for determining the occupancy of the signal in candidate control channels using the measured data. The platform incorporates the proposed DVM-based DCI detection method to enhance reliability and adaptability according to the received signal strength. Finally, it was shown that the difference in RBU between the analyzed results from the platform and the results provided by the mobile service operator is only 0.28% under the same observation conditions. Currently, we are developing real-time hardware based on the proposed algorithm to directly detect the valid DCIs from the captured control channel signal. It is expected that although 5G has recently emerged, the platform will be exploited for cell analysis and forecasting for frequency supply and demand management, given that traffic will be mainly attributed to 4G for the time being. Furthermore, analysis and prediction studies using the collected big data and machine learning-based techniques will be considered in further work.

ACKNOWLEDGMENTS

This work was supported by an Institute of Information & Communications Technology Planning & Evaluation (IITP) grant funded by the Korea government (MSIT) (2017-0-00109, Development of Frequency Analysis Technology for the Virtuous Circulation of Radio Resource).

NOMENCLATURE

$N_{\text{Group}}^{\text{PHICH}}$ Number of PHICH groups
N_{H} PHICH group scaling factor
$N_{\text{RB}}^{\text{BW}}$ Number of total RBs for the bandwidth
N_{CCE} Number of CCEs in a subframe
N_{Sym} Number of OFDM symbols in the control region
$N_{\text{CRS}}^{\text{AP}}$ Number of resource elements for the common reference signal in the control region depending on the number of antenna ports
N_{PDCCH} Number of PDCCHs in the control region
N_{DEC} Maximum number of trials for decoding DCIs
N_{DCI} Number of candidate DCI formats
λ_{CCE} Decision criterion for CCE occupancy
$s_{j,k}$ Received complex symbol on the kth RE among the resources for the jth candidate DCI format
$\tilde{x}_{j,k}^{*}$ Modulated complex symbol of re-encoded DCI bits on the kth RE among the resources for the jth candidate DCI format

ORCID

Jungsun Um https://orcid.org/0000-0003-1514-0500
Igor Kim https://orcid.org/0000-0002-8954-8675
Seungkeun Park https://orcid.org/0000-0003-4956-8775

REFERENCES

1. M. Shafi et al., *5G: A tutorial overview of standards, trails, challenges, deployment and practice*, IEEE J. Sel. Areas Commun. **35** (2017), no. 6, 1201–1221.
2. Cisco, *Cisco Visual Networking Index: forecast and trends 2017–2022*, Cisco White Paper, 2019.
3. J. Guey et al., *On 5G radio access architecture and technology [Industry Perspectives]*, IEEE. Wirel. Commun. **22** (2015), no. 5, 2–5.
4. O. Yilmax, O. Teyeb, and A. Orsino, *Overview of LTE-NR dual connectivity*, IEEE Commun. Mag. **57** (2019), no. 6, 138–144.
5. Evolved universal Terrestrial Radio Access (E-UTRA); Physical layer procedures; (Release 12), 3GPP, TR36.213 v12.1.0, 2013.
6. J. Jeon, *NR wide bandwidth operations*, IEEE Commun. Mag. **56** (2018), no. 3, 42–46.
7. E. Pateromickelakis et al., *LAA as a key enabler in slice-aware 5G RAN: Challenges and opportunities*, IEEE Commun. Stand. Mag. **2** (2018), no. 1, 29–35.
8. A. Astaneh and S. Gheisari, *Review and comparison of routing metrics in cognitive radio networks*, Emerg. Sci. J. **2** (2018), no. 4, 191–201.
9. M. Bichlera, V. Gretschkob, and M. Janssen, *Bargaining in spectrum auctions: A review of the german auction in 2015*, Telecommun. Policy **41** (2017), no. 5–6, 325–340.
10. Y. Chen, L. Duan, and Q. Zhang, *Financial analysis of 4G network deployment*, in Proc. IEEE Conf. Comput. Commun. (Hong Kong) 2015, pp. 1607–1615.
11. S. Yang and L. Hanzo, *Fifty years of MIMO detection: The road to large-scale MIMOs*, IEEE Commun. Surv. Tutor. **17** (2015), no. 4, 1941–1988.
12. G. Y. Li et al., *Multi-cell coordinated scheduling and MIMO in LTE*, IEEE Commun. Surv. Tutor. **16** (2014), no. 2, 761–775.
13. R. Liao et al., *MU-MIMO MAC protocols for wireless local area networks: A survey*, IEEE Commun. Surv. Tutor. **18** (2016), no. 1, 162–183.
14. R. Mostafa et al., *Closed-loop transmit diversity techniques for small wireless terminals and their performance assessment in a flat fading channel*, ETRI J. **34** (2012), no. 3, 319–329.

15. C. Xu et al., *Two decades of MIMO design tradeoffs and reduced-complexity MIMO detection in near-capacity systems*, IEEE Access **5** (2017), 18564–18632.
16. T. Nakamura et al., *Trends in small cell enhancements in LTE advanced*, IEEE Commun. Mag. **51** (2013), no. 2, 98–105.
17. RCRWireless reports, *Small cells and network densification: Policy, spectrum, fiber and mobile networks*, July 2019, available at https://www.rcrwireless.com/.
18. RCRWireless Reports, *Small cell testing update: Getting small cell networks right*, Feb. 2016, available at https://www.rcrwireless.com/.
19. Q. Ye et al., *User association for load balancing in heterogeneous cellular networks*, IEEE Trans. Wireless Commun. **12** (2013), no. 6, 2706–2716.
20. S. Park et al., *An evaluation methodology for spectrum usage in LTE-A networks: Traffic volume and resource utilization perspective*, IEEE Access **7** (2019), 67863–67873.
21. A. Mavrogiorgou et al., *Internet of Medical Things (IoMT): Acquiring and transforming data into HL7 FHIR through 5G network slicing*, Emerg. Sci. J. **3** (2019), no. 2, 64–77.
22. D. S. Kalistratov, *Wireless video monitoring of the megacities transport infrastructure*, Civil Emerg. J. **5** (2019), no. 5, 1033–1040.
23. P. Si et al., *Optimal cooperative internetwork spectrum sharing for cognitive radio systems with spectrum pooling*, IEEE Trans. Veh. Technol. **59** (2010), no. 4, 1760–1768.
24. A. Čokl et al., *Stink bug communication with multimodal signals transmitted through air and substrate*, Emerg. Sci. J. **3** (2019), no. 6, 407–424.
25. K. Javadi and N. Komjani, *Investigation into low SAR PIFA antenna and design a very low SAR U-slot antenna using frequency selective surface for cell-phones and wearable applications*, Ital. J. Sci. Eng. **1** (2017), no. 6, 145–157.
26. J. Um, I. Kim, and S. Park, *Implementation of platform for measurement and analysis on LTE traffic and radio resource utilization*, in Proc. IEEE Int. Conf. Consumer Electron. (Las Vegas, NV, USA), Jan. 2019, pp.1–2.
27. S. Kumar et al., *LTE radio analytics made easy and accessible*, in Proc. ACM Conf. SIGCOMM (Chicago, IL, USA), Aug. 2014, pp. 211–222.
28. R. Falkenberg, C. Ide, and C. Wietfeld, *Client-based control channel analysis for connectivity estimation in LTE networks*, in Proc. IEEE Veh. Technol. Conf. (Montreal, Canada), Sept. 2016, 2016, pp. 1–6.
29. B. Nicola and W. Joerg, *OWL a reliable online watcher for LTE control channel measurements*, in Proc. Annu. Int. Conf. Mobile Comput. Netw. (New York, NY, USA), Oct. 2016, pp. 25–30
30. Keysight Brochure, *89600 WLA software*, available at https://www.literature.cdn.keysight.com/.
31. Rohde & Schwarz Brochure, *TSME Ultracompact Drive Test Scanner*, available at https://www.rohde-schwarz.com/brochure-datasheet/tsme/.
32. S. Sesia, I. Toufik, and M. Baker, *LTE-the UMTS long term evolution: From theory to practice*, 2nd ed, John Wiley & Sons Ltd., UK, 2011.
33. Evolved Universal Terrestrial Radio Access (E-UTRA); Multiplexing and channel coding; (Release 12), TR36.212 v12.1.0, 2013.
34. F. C. Robey et al., *A CFAR adaptive matched filter detector*, IEEE Trans. Aerosp. Electron. Syst. **28** (1992), no. 1, 208–216.
35. A. Mashhour and A. Borjak, *A method for computing error vector magnitude in GSM EDGE systems-simulation results*, IEEE Commun. Lett. **5** (2001), no. 3, 88–91.

AUTHOR BIOGRAPHIES

Jungsun Um received his BS and MS degrees in electronic and electrical engineering from Sungkyunkwan University, Suwon, Republic of Korea, in 2004 and 2006, respectively, and his PhD degree in electrical engineering from the Korea Advanced Institute of Science and Technology, Daejeon, Rep. of Korea, in 2017. Since 2006, he has been with the Electronics and Telecommunications Research Institute, Daejeon, Rep. of Korea, where he is now a principal member. His main research interests are spectrum sharing technologies, interference analysis, and wireless communication systems.

Igor Kim received his BS degree in telecommunications and information technology from Tashkent University of Information Technologies, Tashkent, Uzbekistan, in 2005. He received his MS and PhD degrees in information and communication engineering from Yeungnam University, Gyeongbuk, Rep. of Korea, in 2007 and 2012, respectively. He is currently a senior researcher at the Electronics and Telecommunications Research Institute, Daejeon, Rep. of Korea. His research interests include mobility management, QoS provisioning, interference and resource control in wireless networks, and network simulation study.

Seungkeun Park received his BS and MS degrees in applied statistics from Korea University, Seoul, Rep. of Korea, in 1991 and 1993, respectively, and his PhD degree in information communication engineering from the University of Chungbuk, Cheongju-si, Rep. of Korea, in 2004. He is currently a principal member of the Electronics and Telecommunications Research Institute, Daejeon, Rep. of Korea. His current research interests include communication theory and spectrum management.